Centre for
Automotive Safety Research

Further analysis of the impact characteristics of the New Zealand Fisheries sea lion exclusion device stainless steel grid

G Ponte, A van den Berg, RWG Anderson

Final Research Report for Ministry of Fisheries project SRP2010-05

September 2011

THE UNIVERSITY
of ADELAIDE

Report documentation

DATE

September 2011

PAGES

36

TITLE

Further analysis of the impact characteristics of the New Zealand Fisheries sea lion exclusion device stainless steel grid: Final Research Report for Ministry of Fisheries project SRP2010-05

AUTHORS

G Ponte, A van den Berg, RWG Anderson

PERFORMING ORGANISATION

Centre for Automotive Safety Research
The University of Adelaide
South Australia 5005
AUSTRALIA

SPONSORED BY

Ministry of Fisheries
P.O. Box 1020
Wellington

AVAILABLE FROM

Centre for Automotive Safety Research
http://casr.adelaide.edu.au/publications/researchreports

KEYWORDS

Sea Lion Exclusion Device, Impact Testing, Head Injury

Summary

This report documents the test methods, results and analysis used to create a 'map' of mild traumatic brain injury risk to sea lions interacting with the grid component of the Sea Lion Exclusion Device (SLED) used in the management of the New Zealand squid fishery.

The risk was estimated by testing each of the grid bars within the area of the grid that could be struck by a sea lion during a trawl. The bars were tested at locations along their length at a consistent speed, impactor mass and impact angle. The impact severity was measured according to the head injury criterion (HIC). The results were generalised using a relationship that related the HIC to the speed and mass of the impact, and these were interpolated between locations tested points using curve fitting.

Injury risk was estimated from information about human head injury risk modified using scaling methods. An injury risk map was generated that estimates the risk at all possible impact locations across the grid. This map can be modified to allow for variations in head impactor mass, impact speed and impact angle.

The results can be used to determine the average impact severity (HIC) and the risk of mild traumatic brain injury (MTBI) at any location, and the average of these across the whole grid, for any set of impact conditions.

Given a head mass of 4.8 kg, impact speed of 6 m/s and an impact angle of 90 degrees to the grid, the average HIC of the grid was 551, corresponding to an average risk MTBI of 18%.

Contents

1 Introduction 1

2 Methods and Materials 2

2.1 Test Series 4

2.2 Test Procedure 5

3 Results 9

3.2 Impacts and an angle ϕ to the plane of the grid 14

3.3 Impacts offset from the centreline of the bar 15

3.4 Impacts at compound angles to a grid bar 15

3.5 Multiple Bar Impacts 16

3.6 Angled Impacts to the Horizontal Bar (Bar 12) 16

3.7 Angled Impacts to the Bar 12/Bar 13 17

4 Estimating the risk of Mild Traumatic Brain Injury 18

5 Validation of Offset Equations and Impact Angle Equations 19

5.1 Offset Impact Validation 19

5.2 Validation of scaled severity for an impact occurring at an angle ϕ 19

5.3 Proposed Scaling Function 20

6 HIC and Risk Maps based on the interpolation of test results for variations in parameters m, v and ϕ. 22

7 Summarising the Risk 28

8 Discussion 29

Acknowledgements 31

References 32

1 Introduction

This report is a follow up to an initial report by the Centre for Automotive Safety Research: "Investigation of the impact characteristics of the New Zealand Fisheries Sea Lion Exclusion Device (SLED)" (Ponte et al., 2010). This report was reviewed by Banerjee (2011), and was discussed at a meeting with the Aquatic Environment Working Group in Wellington on 17 May 2011. The meeting recommended further testing and analysis, to provide an estimate of the average risk of mild traumatic brain injury (MTBI) posed by the grid to sea lions that interact with the SLED during trawl operations.

The purpose of the study reported here was to analyse the impact characteristics of a typical SLED grid by conducting a more comprehensive series of tests that would then be used to 'map' the injury risk across the grid.

Ponte et al (2010) describes the background to the test tools used and the injury criteria used in the present tests and analysis, and the reader is referred to that report for more detailed information on these aspects of the study.

This report documents the methods used to expand the previous analysis of the SLED grid. A series of tests at pre-defined locations on each of the grid bars were used to fit functions that could used to interpolate results across the impact area of the grid. Various assumptions were made to account for oblique impacts and validation of some of the derived functions was undertaken.

This report is accompanied by a spreadsheet, which uses the results and functions derived from the testing to calculate the risk across the grid. Changes can be made to variables representing the impact speed, impact angle and impactor mass, to produce estimates of impact severity and injury risk posed by the grid in interactions with a sea lion.

2 Methods and Materials

The grid supplied for the testing is shown in Figure 2-1. It consisted of halves joined by two hammerlocks and a rope that bound the two grid segments tightly at the centre of the grid. It should be noted at the outset that the use of lashing measurably affected the results of the testing – the tight coupling of each half increased the stiffness of the grid in this area. Each half consisted of nine vertical bars, welded to an outer frame. The outer frame consisted of a horizontal bar, two vertical sidebars and an arched bar. The SLED grid was built from 25 mm diameter solid stainless steel. The vertical bars were spaced approximately 200 mm apart (225 mm between bar centres). The gap between the two horizontal was 21 mm. Figure 2-2 shows a scaled schematic drawing of the SLED grid, and a bar numbering system that is used throughout this report.

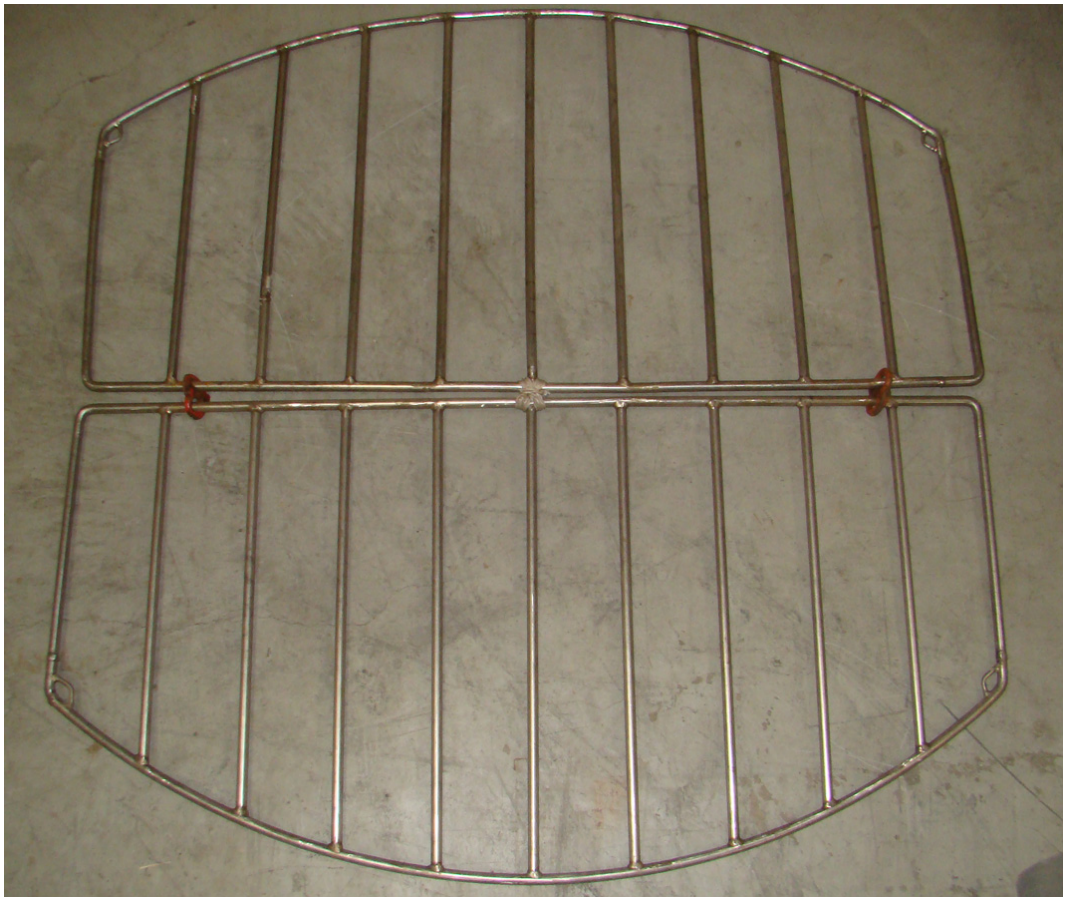

Figure 2-1
A photograph of the supplied grid, with the two hammerlocks and central rope tether

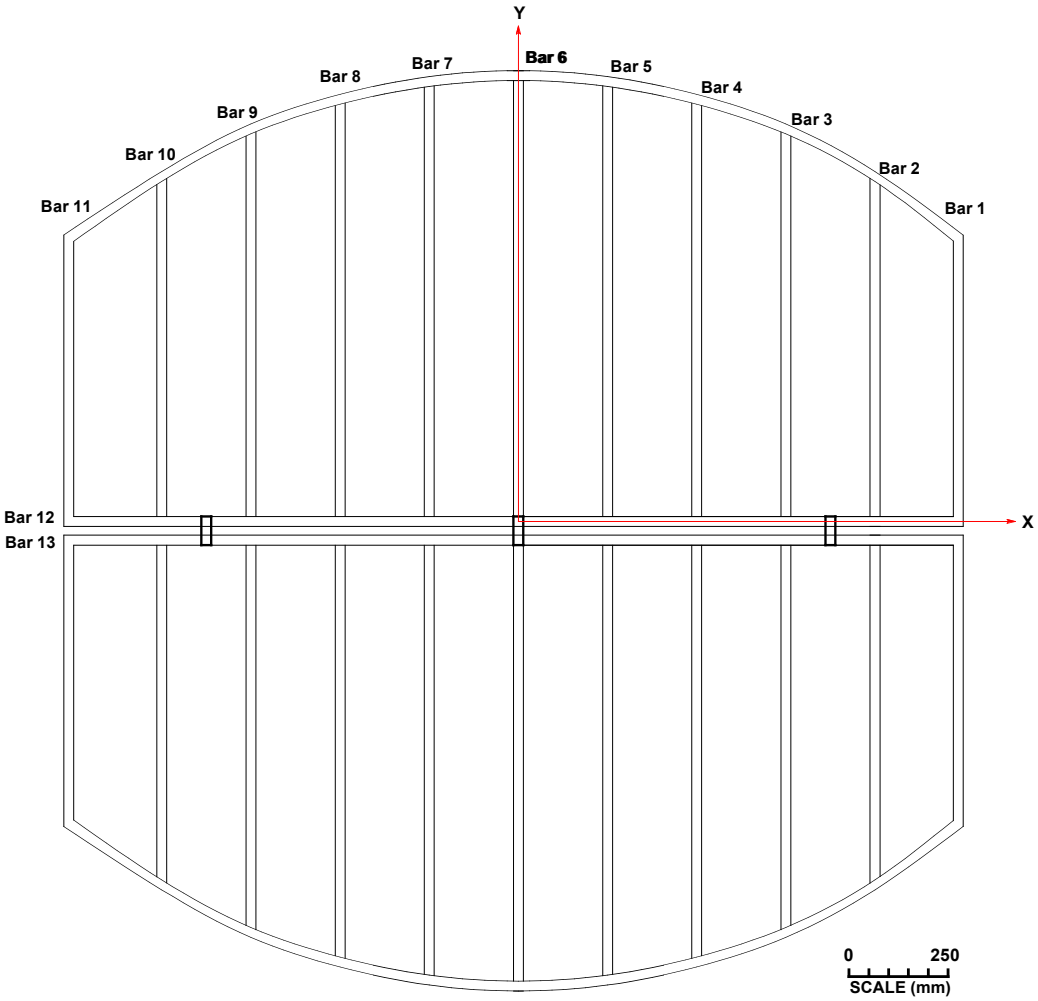

Figure 2-2
Schematic drawing of the NZ SLED Grid

2.1 Test Series

Three series of tests were conducted. The first series of tests were conducted perpendicular and through the centre of each bar at the particular locations “A” to “W” shown in Figure 2-3. The second series of tests were conducted at 60 degrees and 45 degrees though the centre of a bar 6 at location “K”. The third series of tests were perpendicular, but offset by 25mm, 50mm and 75mm from the centre of bar 3 at location “N”. The X-axis runs horizontally along the grid through the centreline of Bar 12, and the Y-axis runs vertically along the grid, through the centreline of Bar 6.

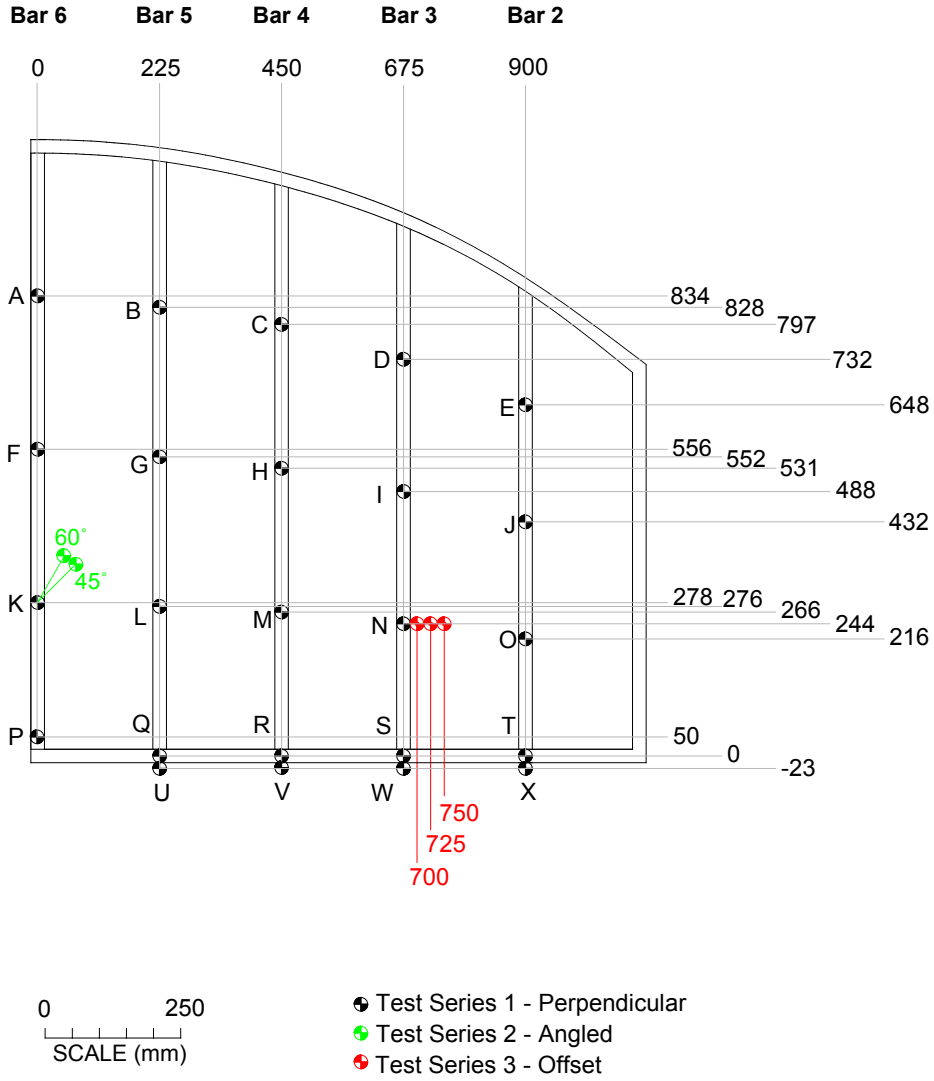

Figure 2-3
A schematic drawing of a quarter of the SLED Grid with the test locations shown (note: Locations marked “U”, “V”, “W” and “X” correspond to the centre-line of the gap between the two horizontal bars of the grid)

Each of the impacts was conducted at 6.0 m/s with the 4.8 kg spherical impactor (see Ponte et al, 2010 for details about the impactor).

2.2 Test Procedure

2.2.1 Series 1 Tests

All impact tests in series 1 were conducted perpendicular to the grid (i.e. at an impact angle of 90 degrees) and at an impact speed of 6 m/s as shown in Figure 2-4 and Figure 2-5.

Bar 12 was tested at each intersection of a vertical bar, except at the grid origin (0,0), where the rope tether was located - no test was performed at this location as it was felt that the rope lashing would cushion the impact, and therefore the result would be of limited value in the interpolation of tests results either side of this location.

The grid was supported around the outer edge of the grid, consistent with the methods used in Ponte et al. (2010). This condition was judged best to simulate the tension provided by the netting during a trawl. In some cases, support at the end of the bar being tested was achieved through a moveable hydraulic bottle jack as shown in Figure 2-5. Note also in Figure 2-5 the distortion across the horizontal bar. This distortion necessitated the testing of geometrical symmetrical locations on the grid that were undeformed to ensure consistent results.

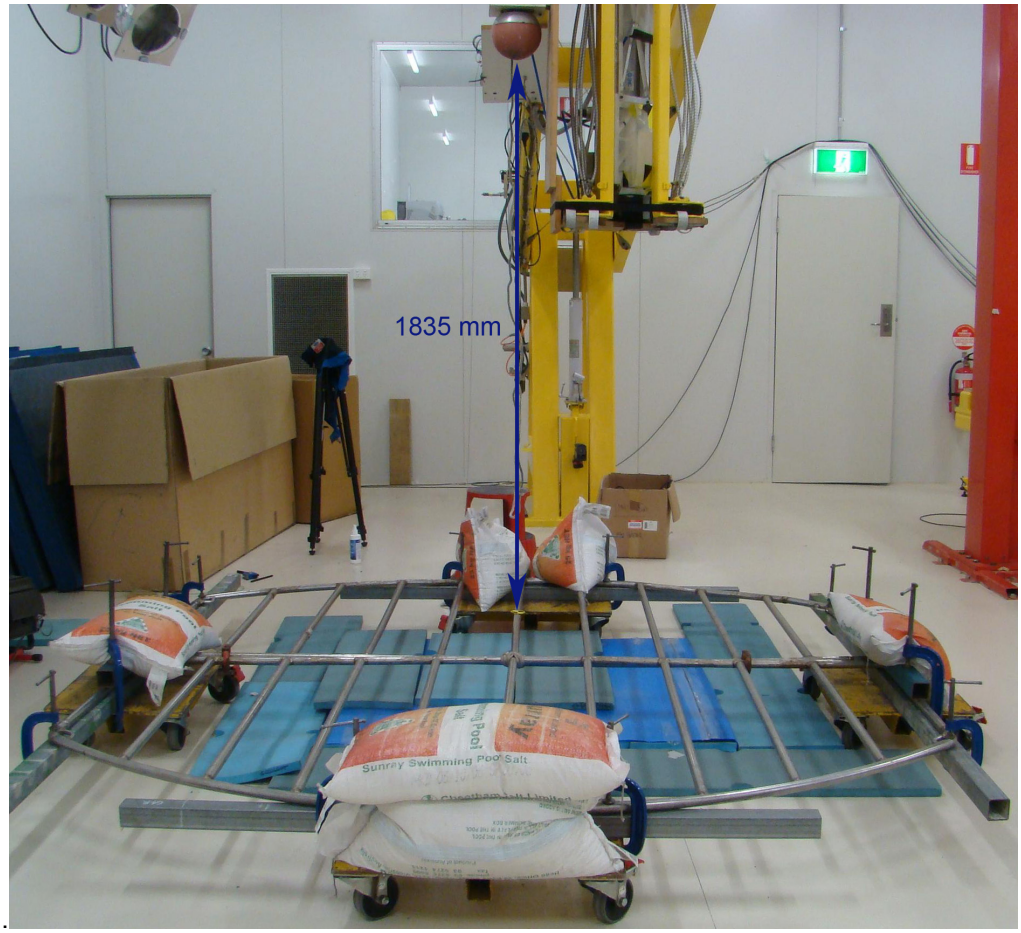

Figure 2-4
Test set-up for the perpendicular drop tests

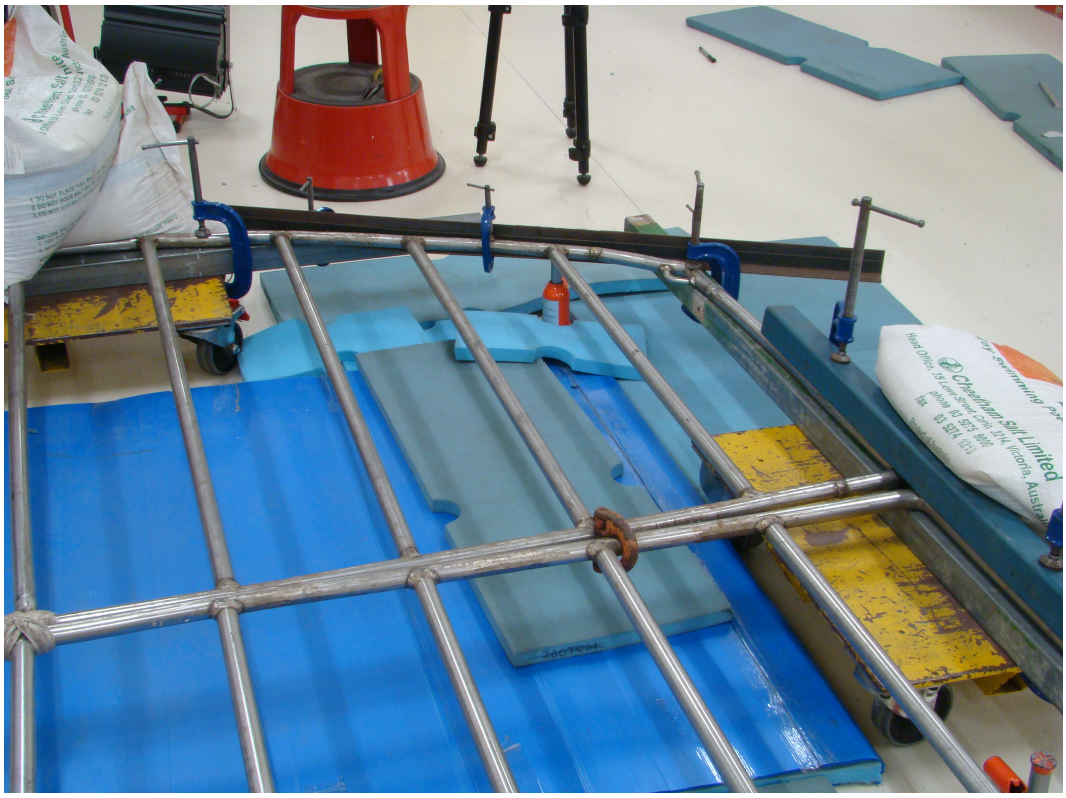

Figure 2-5
Close-up view of the test set-up of the grid, with distortion across the horizontal mid section and the rope tether in the centre of the bar

2.2.2 Series 2 Tests

Three tests were conducted on Bar 6 at location “K” (0,278). These tests were at an impact angle of 90 degrees, 60 degrees and 45 degrees as shown in Figure 2-6 and Figure 2-7. The purpose of this testing was to evaluate the difference in impact angle on HIC for the same impactor mass and impact speed, essentially to examine the effect of angled glancing blows. The tests were required to validate hypotheses regarding the use of the normal velocity to scale the severity in angled impacts.

In these angled impact tests, one half of the grid was held up rigidly at the centre of bar 6. The grid angle and drop height were adjusted so that in each test, the location tested was the first point of contact between the head impactor and the grid bar at the required speed of 6.0 m/s.

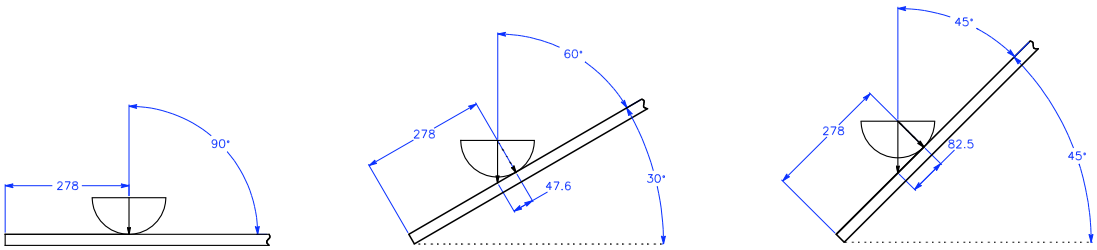

Figure 2-6
The impact angle configurations for bar 6 on the grid

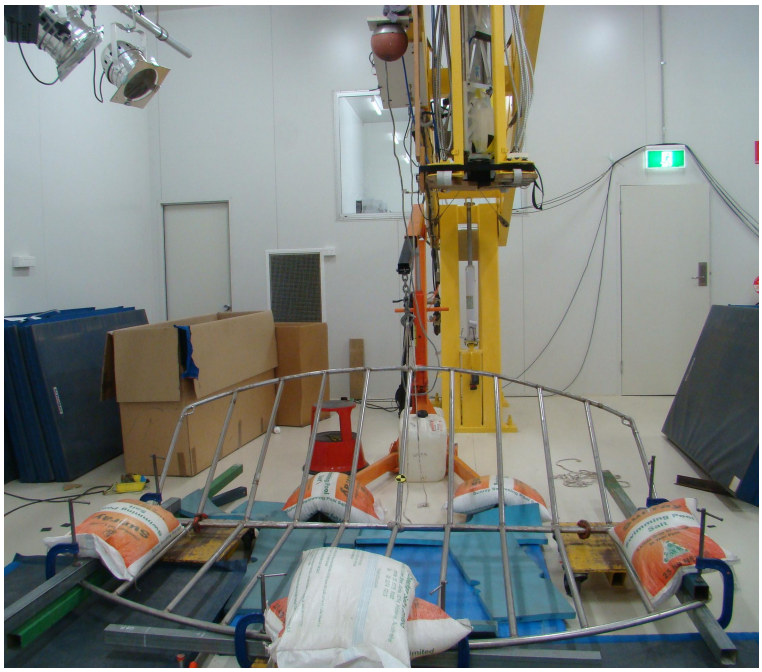

Figure 2-7
Test set-up for varied impact angle tests

2.2.3 Series 3 Tests

On Bar 3, at location “N” (675, 244), impacts between the head impactor and the grid bar were conducted at 25 mm, 50 mm and 75 mm offsets as shown in Figure 2-8. This was done to examine the effect of offset glancing blows with each grid bar.

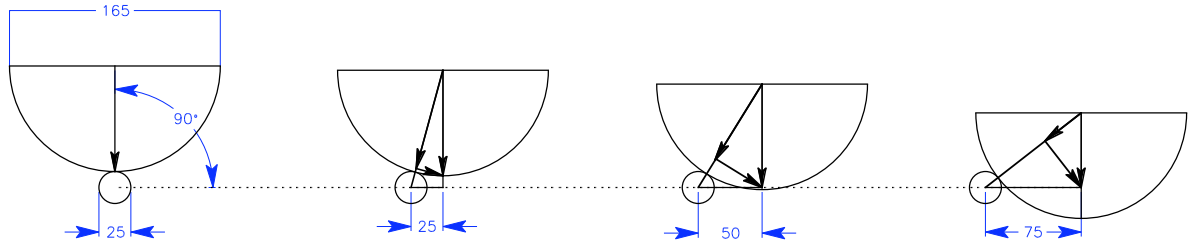

Figure 2-8
Impact configurations for bar 3 offset impacts (looking through the cross section of the bar)

2.2.4 Interpolation

The results from the perpendicular impacts on each grid bar in Test Series 1 were plotted against the longitudinal position of the test on the relevant bar of the grid. These points were then fitted with an appropriate polynomial function. From this process, functions were derived to represent the HIC under

the specific test conditions based on impact location. These functions were assumed to be indicative of the mechanical response for a particular grid bar within the impact area for a particular bar.

These individual functions will be combined with scaling methods described in the proceeding sections of this report and used in Ponte et al (2010), to take into account variations in the impact mass and impact speed.

To take into account both variations in impact angle, and impacts that are off-set from the centreline of each bar, further modifying functions were derived in consideration of this. The objective of these calculations was to take into account the variability in the impact conditions that may be possible in interactions between the sea lion population and the grid.

3 Results

The following tables summarise the results of the testing. The head injury criterion was calculated for each test. HIC uses information on the impact deceleration of the head impactor to indicate injury severity (see Ponte et al., 2010 for more information).

Table 3.1
Summary of test results for the perpendicular impact tests at 6.0 m/s

Bar 2	Test number	X (mm)	Y (mm)	HIC
	10061106	900	0	1261
	10061104	900	216	893
	10061108	900	432	857
	10061109	900	648	1262
Bar 3	**Test number**	**X (mm)**	**Y (mm)**	**HIC**
	14061103	675	0	810
	14061102	675	244	670
	14061101	675	488	603
	14061100	675	732	944
Bar 4	**Test number**	**X (mm)**	**Y (mm)**	**HIC**
	14061104	450	0	658
	14061105	450	266	629
	14061106	450	531	553
	14061107	450	797	808
Bar 5	**Test number**	**X (mm)**	**Y (mm)**	**HIC**
	15061101	225	0	651
	15061100	225	276	598
	14061109	225	552	501
	14061108	225	828	738
Bar 6	**Test number**	**X (mm)**	**Y (mm)**	**HIC**
	09061103	0	50	915
	09061102	0	278	635
	09061100	0	556	545
	10061100	0	834	927

Table 3.2
Summary of test results for the perpendicular impact tests between the two horizontal centre bars (bar 12 and bar 13) of the grid at 6.0 m/s

	Test number	X (mm)	Y (mm)	HIC
Bar 2	15061105	900	-23	1787
Bar 3	16061102	675	-23	1717
Bar 4	15061103	450	-23	1347
Bar 5	15061104	225	-23	956

Table 3.3
Summary of test results for the angled impact tests on Bar 6 at 6.0 m/s

Bar 6	Test number	X (mm)	Y (mm)	HIC
45 degrees	17061100	0	278	351
60 degrees	17061101	0	278	542
90 degrees	17061102	0	278	675

Table 3.4
Summary of test results for the perpendicular offset impact tests on Bar 3 at 6.0 m/s

Bar 3	Test number	X (mm)	Y (mm)	HIC
0 mm	14061102	675	244	670
25 mm	15061106	700	244	605
50 mm	15061107	725	244	447
75 mm	15061108	750	244	190

A graphical representation of the test results for each of the bars is presented below. The results along each of the bars were adequately represented by a second order polynomial, with the exception of bar 6 where a fourth order polynomial was more appropriate and bar 12/13 which used a combination of a second order polynomial and linear equation. This reflected the influence of the centre binding on the impact characteristics of the grid. It would normally be expected that the centre of the longest bar (bar 6) would be the least injurious on the grid. However, the binding stiffened the grid at this location.

As mentioned previously, there was no test conducted at coordinate locations (0,0) or (0,-23) due to the binding at the centre of the grid. To obtain the HIC at these locations, a fourth order polynomial function for bar 6 was fitted to the test results for bar 6. This included the geometrically symmetrical location on the other grid half at (0,-96) where the symmetrical HIC is 915 as depicted in Figure 3-1 by the open red circle.

The function allowed extrapolation of the HIC at coordinate locations (0,0) and (0,-23), where the HIC was 946 and 951 respectively.

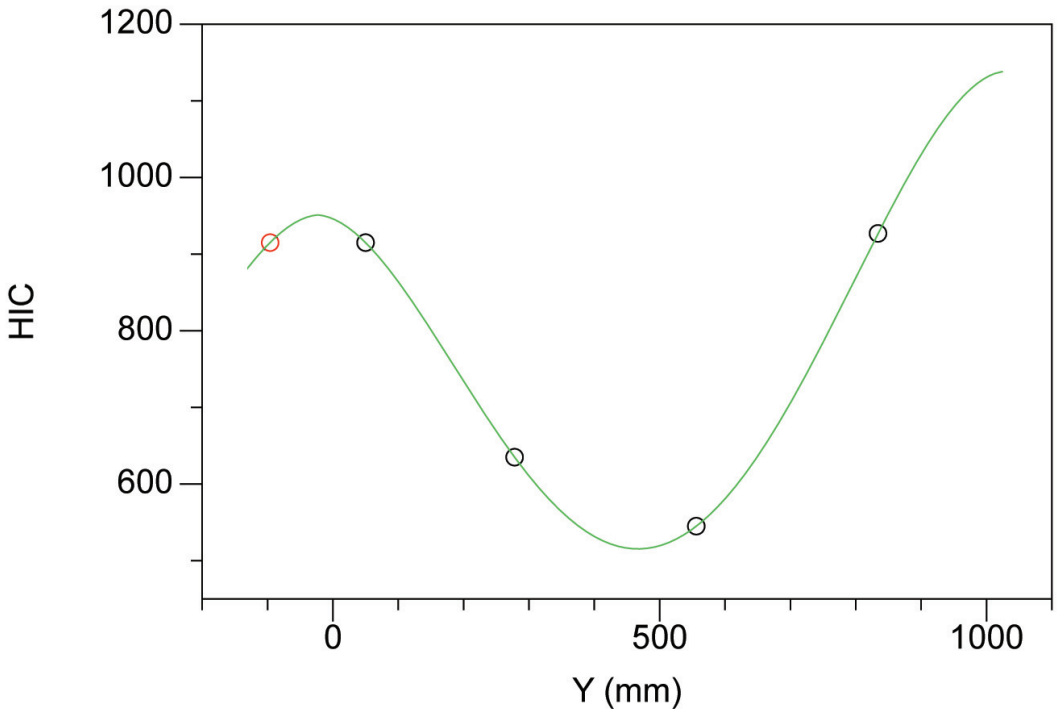

Figure 3-1
The HIC results plotted for the impact tests on Bar 6, extrapolated to include the untested locations (0,0) and (0,-23)

The HIC value at (0,-23) of 951 for bar 6 at was used as the HIC at (0,-23) for bar 12/bar 13. A linear equation was fitted to this HIC result of 951 at point at (0,-23) to the HIC result at (225,-23) at location

“T” where the HIC result was 956. A second order polynomial was then fitted to the HIC results for the actual tests conducted on bar 12/bar 13 as show in Figure 3-2.

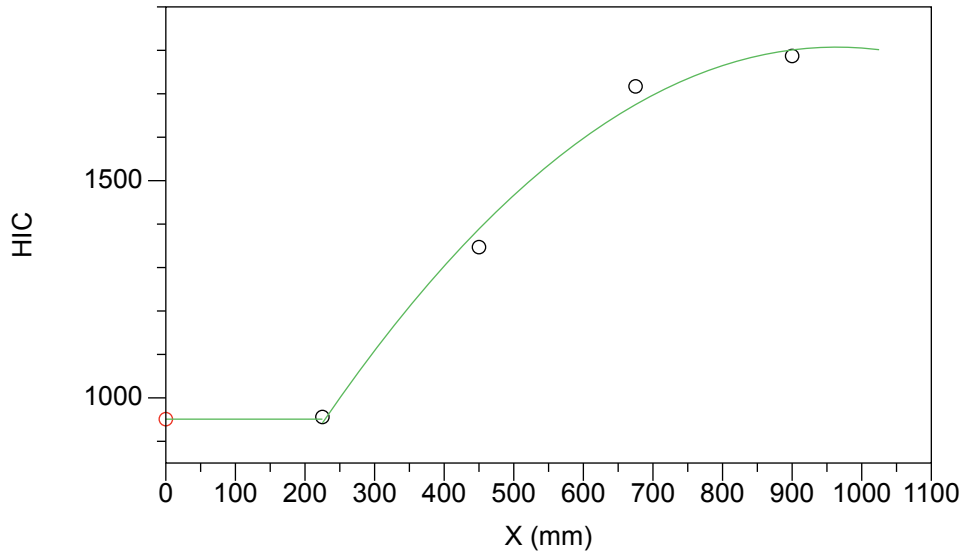

Figure 3-2
The graphed results for bar 12/13. The open red circle was interpolated from the function fitted to the results of Bar 6 (Figure 3-1). The black open circles represent the actual test results for which the second order polynomial is fitted for X>225mm

Figure 3-3, Figure 3-4, Figure 3-5 and Figure 3-6 show the plotted HIC results with corresponding polynomial function lines for bar 12, bar 2, bar 3 and bar 4 respectively.

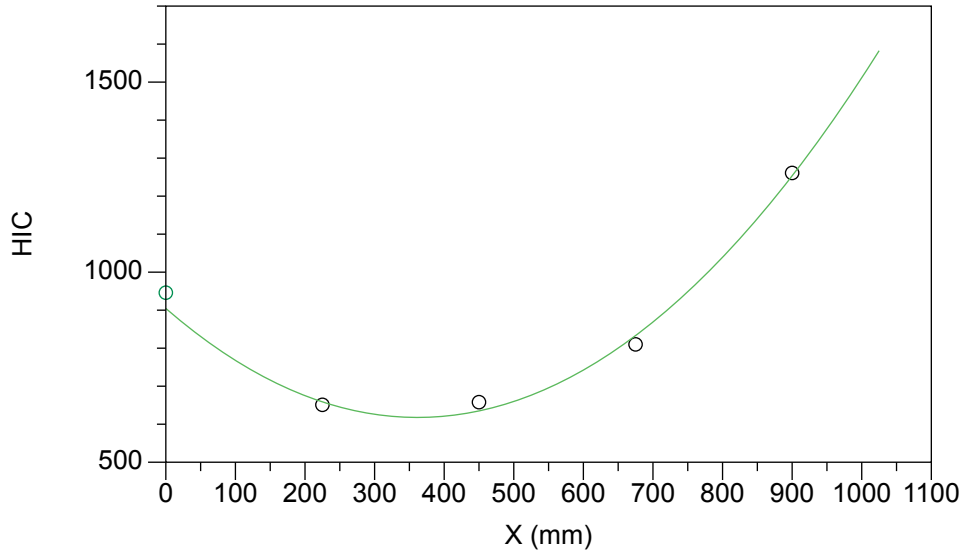

Figure 3-3
Plot of HIC results for bar 12 and corresponding fitted polynomial

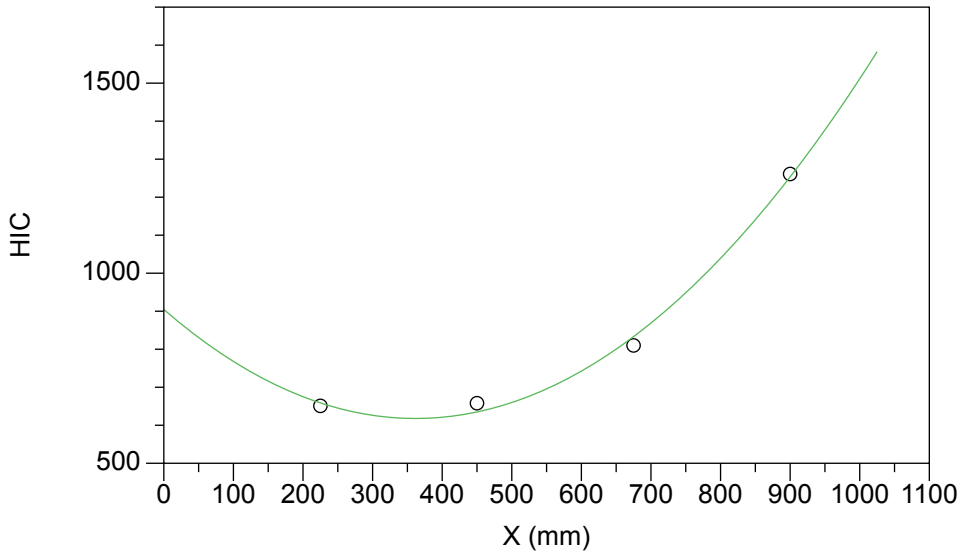

Figure 3-4
Plot of HIC results for bar 2 and corresponding fitted polynomial

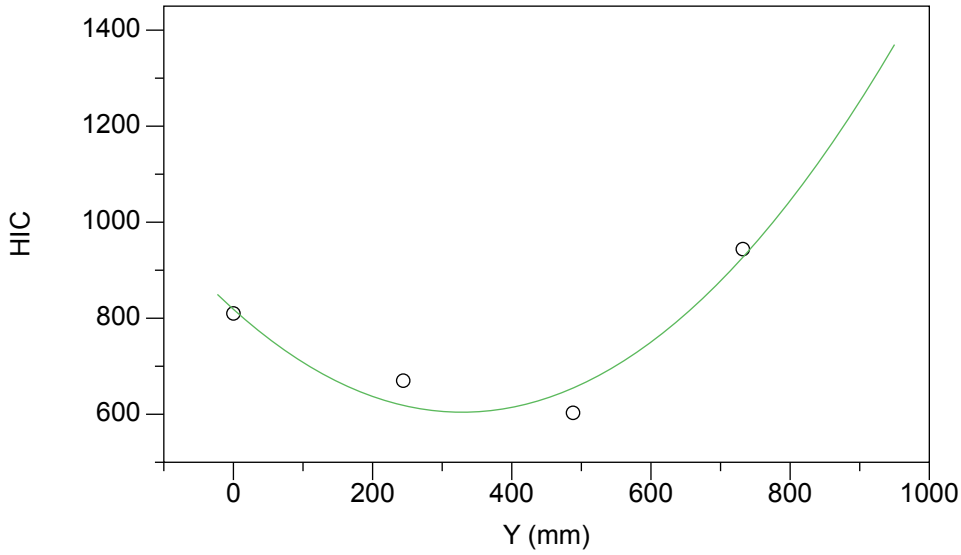

Figure 3-5
Plot of HIC results for Bar 3 and corresponding fitted polynomial

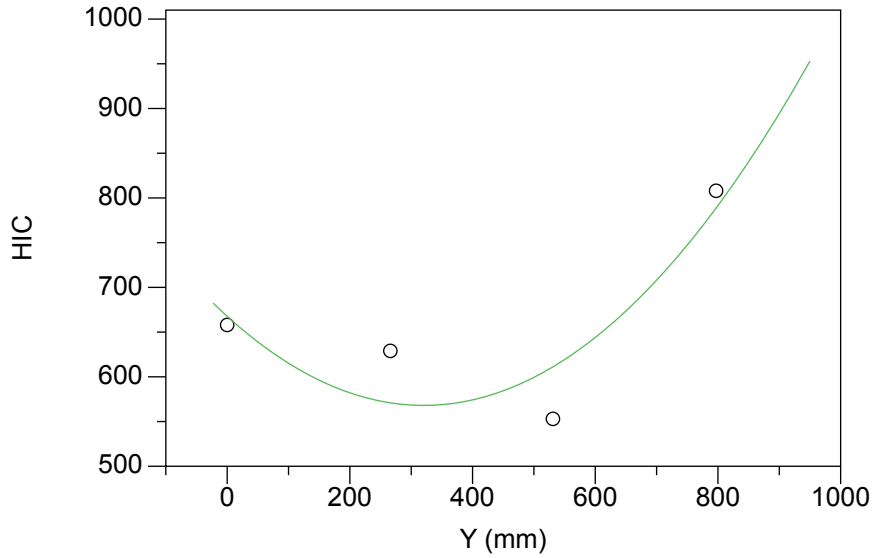

Figure 3-6
Plot of HIC results for bar 4 and corresponding fitted polynomial

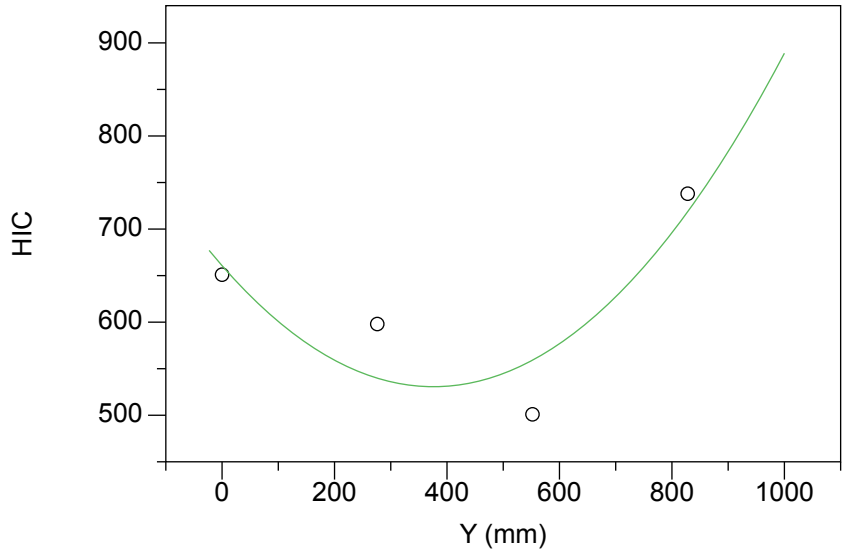

Figure 3-7
Plot of HIC results for bar 5 and corresponding fitted polynomial

It might be noted that the assumption of a second order polynomial is only approximately for bars 4 and 5 in particular. Higher order polynomials did fit the data more closely; however, the use of these higher order functions caused the functions to decrease in the extrapolated regions, toward the arched section of the grid. As this is physically unrealistic, it was judged preferable to maintain an increasing level of severity in this region.

3.1.1 Summary of polynomial functions fitted to each bar

Each of the bars on the grid tested can be represented by a polynomial function, generalised by the following equation:

$$HIC_T = a\lambda^4 + b\lambda^3 + c\lambda^2 + d\lambda + e \qquad \text{Equation 1}$$

Where a,b,c,d and e are the constants obtained from the polynomial functions for each of the bars, and λ is the vertical or horizontal distance along the bar being tested. The resulting equations estimate the HIC in a perpendicular impact

Table 3.5 shows the constants for each bar based on the HIC results in a perpendicular impact with a 4.8 kg head impactor, at 6.0m/s.

Table 3.5
Constants derived from the polynomial function trend lines representing the HIC distributions for each bar

	a	b	c	d	e
Bar 2	0	0	4.14E-03	-2.70E+00	1.27E+03
Bar 3	0	0	2.02E-03	-1.34E+00	8.27E+02
Bar 4	0	0	9.98E-04	-6.52E-01	6.75E+02
Bar 5	0	0	9.52E-04	-7.29E-01	6.70E+02
Bar 6	-6.63E-09	1.30E-05	-5.83E-03	-3.61E-01	9.46E+02
Bar 12	0	0	2.19E-03	-1.59E+00	9.05E+02
Bar 12/13 >225 mm	0	0	-1.59E-03	3.06E+00	3.35E+02
Bar 12/13 <225 mm	0	0	0	2.22E-02	9.51E+02

Scaling methods can be used to estimate the HIC at different speeds and effective head masses. The method is described in Searson (2011). The equation is:

$$HIC_E = HIC_T \times \left(\frac{m}{m_T}\right)^{-3/4} \left(\frac{v}{v_T}\right)^N \qquad \text{Equation 2}$$

Where HIC_E is the estimated HIC value scaled according to the impact conditions mass = m and speed = v, HIC_T is the result from a perpendicular impact test, conducted with a head impactor with a mass m_T at an impact velocity v_T. In a spring like structure N is 2.5 (Searson (2011)). Empirical values for N range between 1.61 and 3.04 (Searson (2011)).

In the present analysis, the test parameters used were: m_T = 4.8 kg and v_T = 6 m/s.

Equation 2 can be rewritten incorporating the test parameters:

$$HIC_E = HIC_T \times \left(\frac{m}{4.8}\right)^{-3/4} \left(\frac{v}{6}\right)^N \qquad \text{Equation 3}$$

3.2 Impacts and an angle ϕ to the plane of the grid

When the impact occurs at an angle to the surface (but in line with the centreline of the bar) Equation 3 can be adjusted:

$$HIC_{\phi} = HIC_T \times \left(\frac{m}{4.8}\right)^{-3/4} \left(\frac{v \sin \phi}{6}\right)^N$$ Equation 4

The validity of this equation is discussed in section 5.

3.3 Impacts offset from the centreline of the bar

For impacts offset from the centre of the bar (a glancing blow), the component impact angle θ, is a function of the offset distance δ, the radius of the head impactor r_h (=82.5mm) and the radius of the impacted grid bar r_b. (=12.5mm), see Figure 2-8.

The following relationships are relevant:

$$\cos(\theta) = \frac{\delta}{r_h + r_b}$$ Equation 5

In the case of the tests conducted at $r_h + r_b = 95$

$$\theta = \arccos\left(\frac{\delta}{95}\right)$$ Equation 6

So for an offset distance δ, and for perpendicular impacts, HIC can be estimated by:

$$HIC_{\delta} = HIC_T \times \left(\frac{m}{4.8}\right)^{-3/4} \left(\frac{v \sin \theta}{6}\right)^N$$ Equation 7

or

$$HIC_{\delta} = HIC_T \times \left(\frac{m}{4.8}\right)^{-3/4} \left(\frac{v \sin\left(\arccos\left(\frac{\delta}{95}\right)\right)}{6}\right)^N$$ Equation 8

3.4 Impacts at compound angles to a grid bar

In the case where the velocity is at some non-perpendicular angle to the plane of the grid, and where the impact is offset from the centreline of the bar, Equation 4 and Equation 8 can be combined:

$$HIC_{\delta,\phi} = HIC_T \times \left(\frac{m}{4.8}\right)^{-3/4} \left(\frac{v \sin \phi \sin\left(\arccos\left(\frac{\delta}{95}\right)\right)}{6}\right)^N$$ Equation 9

3.5 Multiple Bar Impacts

In some locations on the grid, the head impactor would have come into contact with more than one bar simultaneously, and a strategy was required for interpolating the results of tests in these regions. Impacts in the vicinity of the grid corners (within the possible impact area) would result in the simultaneous, or almost simultaneous impact of a horizontal and vertical bar on the grid. A few assumptions were made to handle this situation in the interpolation of the results in these cases.

- For impacts where the offset was equidistant from the vertical bar and horizontal bar (e.g., offset 25 mm, 50 mm or 75 mm from both bars) it was assumed that the bar that produced the highest adjacent HIC would have the most influence on the result. Accordingly, the HIC was determined by the higher of the two HIC values in conjunction with the offset distance. The basis for this assumption was that the stiffness of the higher HIC location would dominate the response.
- Where the impact was closer to one bar than the other bar (e.g. If the impact location was 25 mm from the horizontal bar and 50 mm from the vertical bar), it was assumed that the closer bar would determine the impact severity, as it would be that bar that would make first contact with the head. Accordingly the HIC value was determined from that HIC value in conjunction with the offset distance.

This method effectively assumes that there is only a single impact, and gives a conservative (low) estimate of the HIC result.

3.6 Angled Impacts to the Horizontal Bar (Bar 12)

Impacts in line with the midline of the horizontal bar are affected by the angle of the grid. This effect is described in Ponte et al, (2010).

The results from Ponte et al, (2010) are reproduced in Figure 3-8, with the HIC result for the perpendicular impact being set to unity and the change in HIC expressed as a scaling factor. This scaling factor was applied to the short sections of the horizontal bar (bar 12) when the impact angles were less than 90 degrees (see Figure 3-9).

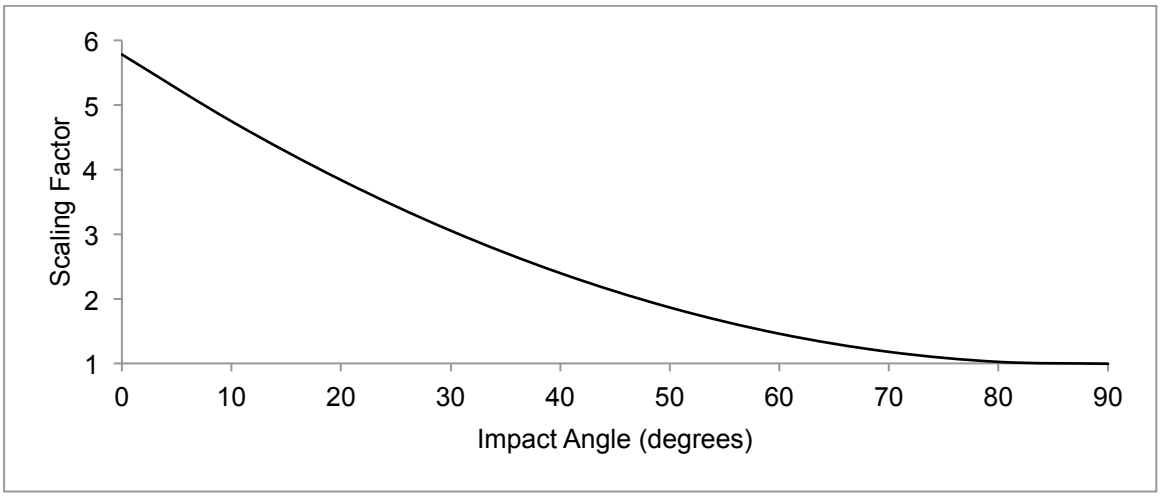

Figure 3-8
The effect of impact angle on HIC along the short horizontal mid section of the grid between two vertical bars

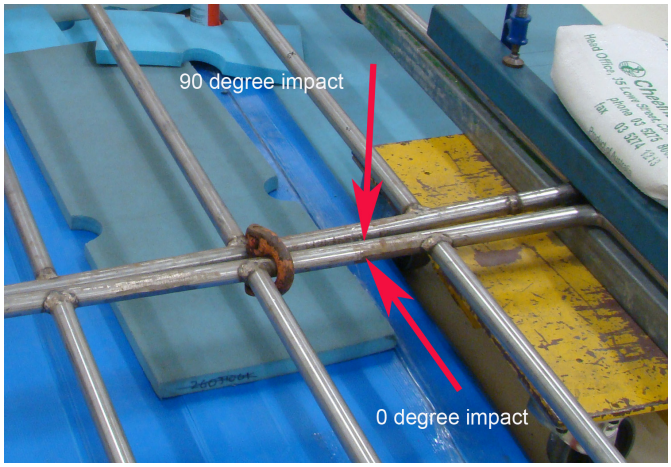

Figure 3-9
Scaling factor applicable to impacts to the short sections of Bar 12 for angles less 90 and greater than 0 degrees

3.7 Angled Impacts to the Bar 12/Bar 13

Impacts perpendicular to Bar 12/Bar 13 involve simultaneous impact with both bar 12 and bar 13. The function estimating HIC for this impact configuration is represented by Equation 1 with the relevant constants from Table 3.5. For impact angles less than 90 degrees, only one bar is struck initially (bar 12), and hence dominates the HIC response for that impact. Consequently, for all impacts on bar 12/bar 13 with an impact angle less than 90 degrees, the function representing bar 12 (and the corresponding relevant constants) is used for these impact configurations.

4 Estimating the risk of Mild Traumatic Brain Injury

In our previous report (Ponte et al., 2010), estimates of the risk for mild traumatic brain injury to a sea lion were presented. These curves are presented in Figure 4-1 below. The reader is referred to our earlier report for a description of these curves. The power scaling relationship refers to possible ways in which injury tolerance might vary with brain mass.

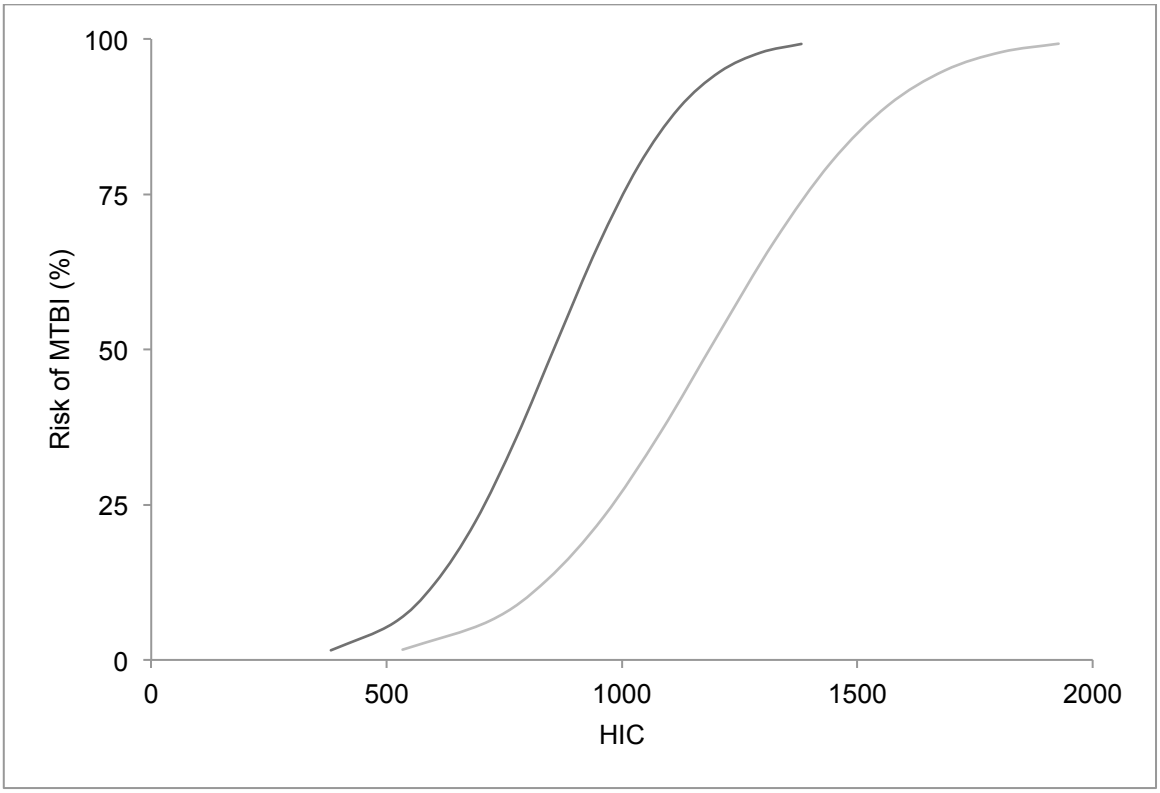

Figure 4-1
Mild traumatic brain Injury risk curves (derived from Funk et al (2007), scaled to estimate tolerance for the sea lion brain injury based on 1/3 power (darker line) and 2/3 power (lighter line) relationships with brain mass

To automate the calculation of MTBI risk, these curves were described by a normal cumulative distribution, i.e.

$$MTBI = \frac{1}{2}\left[1 + erf\left(\frac{x-\mu}{\sqrt{2\sigma^2}}\right)\right]$$

Equation 10

Where x is the calculated HIC at a particular impact location, μ is the mean, and σ is the standard deviation. The values for σ and μ for each curve are 218 and 855 in the case of the curve based on 1/3 power scaling law, and 305 and 1186 in the case of the risk curve based on a 2/3 power scaling law.

5 Validation of Offset Equations and Impact Angle Equations

5.1 Offset Impact Validation

Equation 8 was used to calculate the HIC resulting from the offset impacts (glancing blows). To check it's validity, impact tests were conducted at 25 mm, 50 mm and 75 mm offsets at location "N". A comparison of the actual HIC results to the HICs estimated by Equation 8 and presented in Figure 5-1. Test results are similar to the estimated when N = 2.5. When N is set to 1.9, the HIC is over-estimated. Note, the chart also shows the value at 95 mm offset, where the head impactor just misses the bar resulting in no impact and zero HIC.

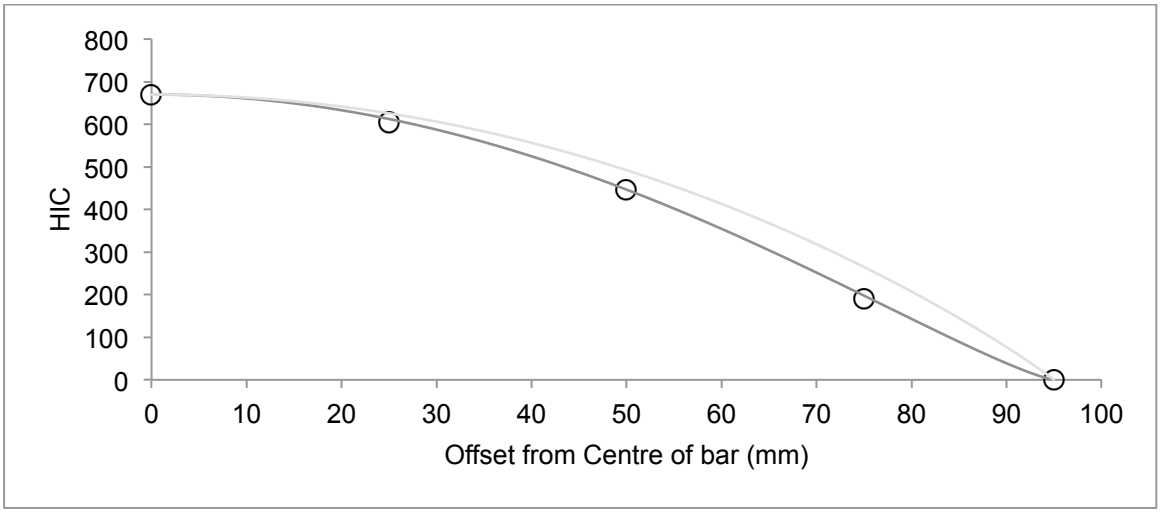

Figure 5-1
Validation of HIC test results against the theoretical calculated offset results

5.2 Validation of scaled severity for an impact occurring at an angle ϕ

Several impact tests were conducted as discussed in section 2.2.2, to test our assumption about how HIC should be scaled for non perpendicular impacts. For each test, the result was estimated from the perpendicular test and Equation 4. A comparison of the actual HIC results to the calculated HIC results are presented in Figure 5-2.

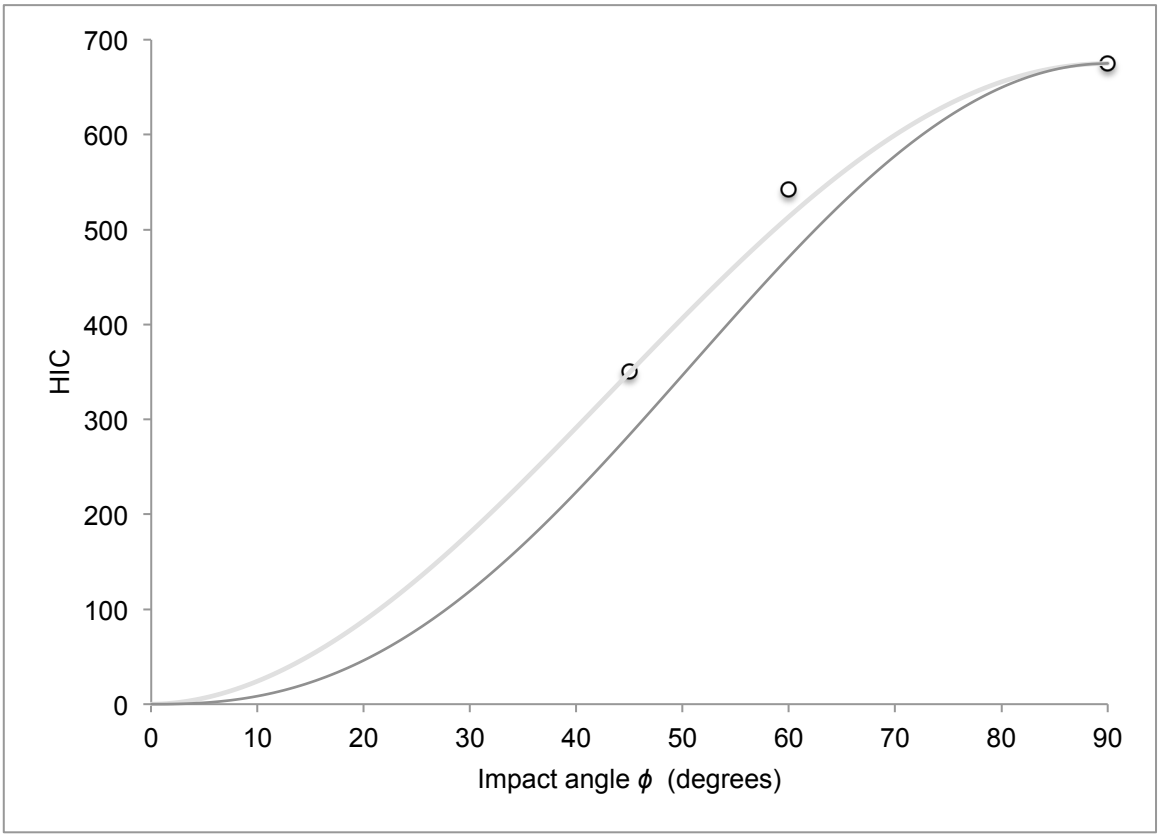

Figure 5-2
Variation in HIC according to impact angle on a vertical bar at location "K" on bar 6. The test data is represented by the black open circles, the light grey and dark grey lines represent the functions that describe the HIC variation by impact angle for N=1.9 and 2.5 respectively

The original version of Equation 2 presented in Searson (2011), proposed a value N = 2.5 for scaling HIC. This exponent seems to be most appropriate for perpendicular impacts, but tends to under estimate the HIC for impact angles less than 90 degrees compared to the impact test result. It was found that using N = 1.9, gave a calculation of HIC closer to the impact test results for the same angle, with the 4.8 kg head impactor.

It is probable that the reason that the HICs were higher than those estimated, given N = 2.5, is the contribution of friction in an angled impact. In a perpendicular impact the effect of friction does not affect the HIC, however for non perpendicular impact angles, the effect of friction is likely to influence the HIC result, as it will cause additional deceleration.

We don't know how the friction in our tests compare with the friction in interactions with a sea lion. For this reason, we proposed a range for N between 1.9 and 2.5, so the effects of our assumptions about friction, and hence N, on the overall risk posed by the grid can be checked.

5.3 Proposed Scaling Function

For an impact with a spring type model, Equation 9 can be rewritten as shown in Equation 11, for $N_1 = N_2 = N$. However, according to the validation tests a better estimate of HIC based on impact angle and offset may be represented by Equation 11, with $N_1 = 1.9$ and $N_2 = 2.5$ respectively.

$$HIC_{\delta,\phi} = HIC_T \times \left(\frac{m}{4.8}\right)^{-3/4} (\sin \emptyset)^{N_1} \left(\frac{v \sin\left(\arccos\left(\frac{\delta}{95}\right)\right)}{6}\right)^{N_2}$$

Equation 11

As mentioned in section in 5.2, if the effect of friction in the laboratory tests is over estimating the HIC, then despite the validation tests indicating that N_1 should be set to 1.9, Equation 11 allows N_1 to be set to 2.5 if necessary, to check the effect on average risk of MTBI.

6 HIC and Risk Maps based on the interpolation of test results for variations in parameters m, v and ϕ.

The objective of this stage of the modelling was to put together each of the equations relevant to teach of the individual bars of the grid into a form that would show estimates of severity for all possible impact locations and the variation of the results for any values of the represent the head mass, impact speed, impact angle and the factor that is used to relate severity to impact speed.

The total grid impact area was discretised into a map of 25 mm x 25 mm cells, 4947 cells in all. This area represents the area of the grid that can be struck by the centre of the 165 mm head impactor without obstruction (that is a clear impact with the grid within the bounds of the netting).

The interpolation functions and the adjustments to HIC described by Equation 1 to Equation 8 and sections 3.5 and 3.6 were applied to each of these individual cells. These cells were incorporated into a Microsoft Excel workbook with consideration to all the test parameters:

- Test head impactor mass (nominally 4.8 kg)
- Test impact speed (nominally 6.0 m/s)
- Test impact angle (nominally 90 degrees)

With adjustment for the global parameters:

- Head mass, m
- Relative Impact speed with grid, v
- Impact Angle with the plane of the grid, ϕ
- Sea Lion Mild Traumatic Brain Injury Tolerance
    - 1 for low tolerance to injury using 1/3 power scaling law
    - 2 for high tolerance to injury using 2/3 power scaling law

Offset distance from the centreline of each bar is incorporated into the calculations that apply to the relevant cells.

Figure 6-1 is the HIC map for a quarter of the grid, showing the individual HIC results predicted by the derived functions when m, v, ϕ are set to the actual test conditions.

The colour coding is based on HIC ranges shown in Table 6.1.

Table 6.1
HIC ranges and colour codes

0 < HIC < 332	
333 < HIC < 666	
HIC > 667	

Figure 6-2 is a map of MTBI risk for a quarter section of the grid, when m, v, ϕ correspond to the actual test conditions used. Here, risk is defined according to the curve scaled from human tolerance using a 1/3 power scaling law. The transitioning colour code for the MTBI risk is shown in Table 6.2, and can be used as an indicator of injury risk 'hot spots'.

Figure 6-3 and Figure 6-4 show the Grid HIC map and MTBI map, respectively for an impact where m and v are set to the actual test conditions and ϕ is 45 degrees. In this configuration, injury risk is concentrated around the horizontal bar.

Table 6.2
MTBI Risk and colour codes

0%
25%
50%
100%

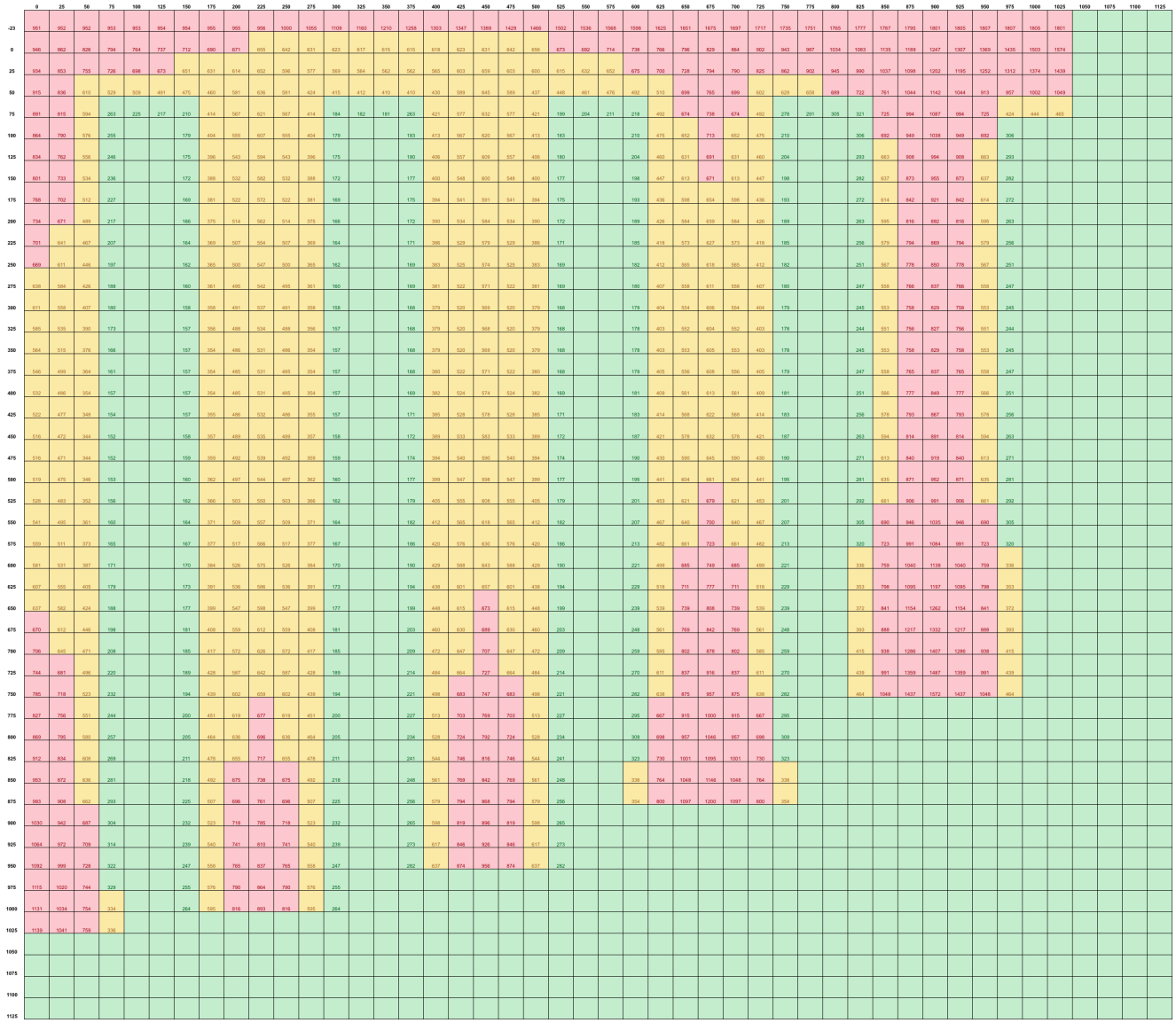

Figure 6-1
HIC map for the Grid, based on actual test conditions, impact angle 90 degrees, impact speed 6.0 m/s, head mass 4.8 kg

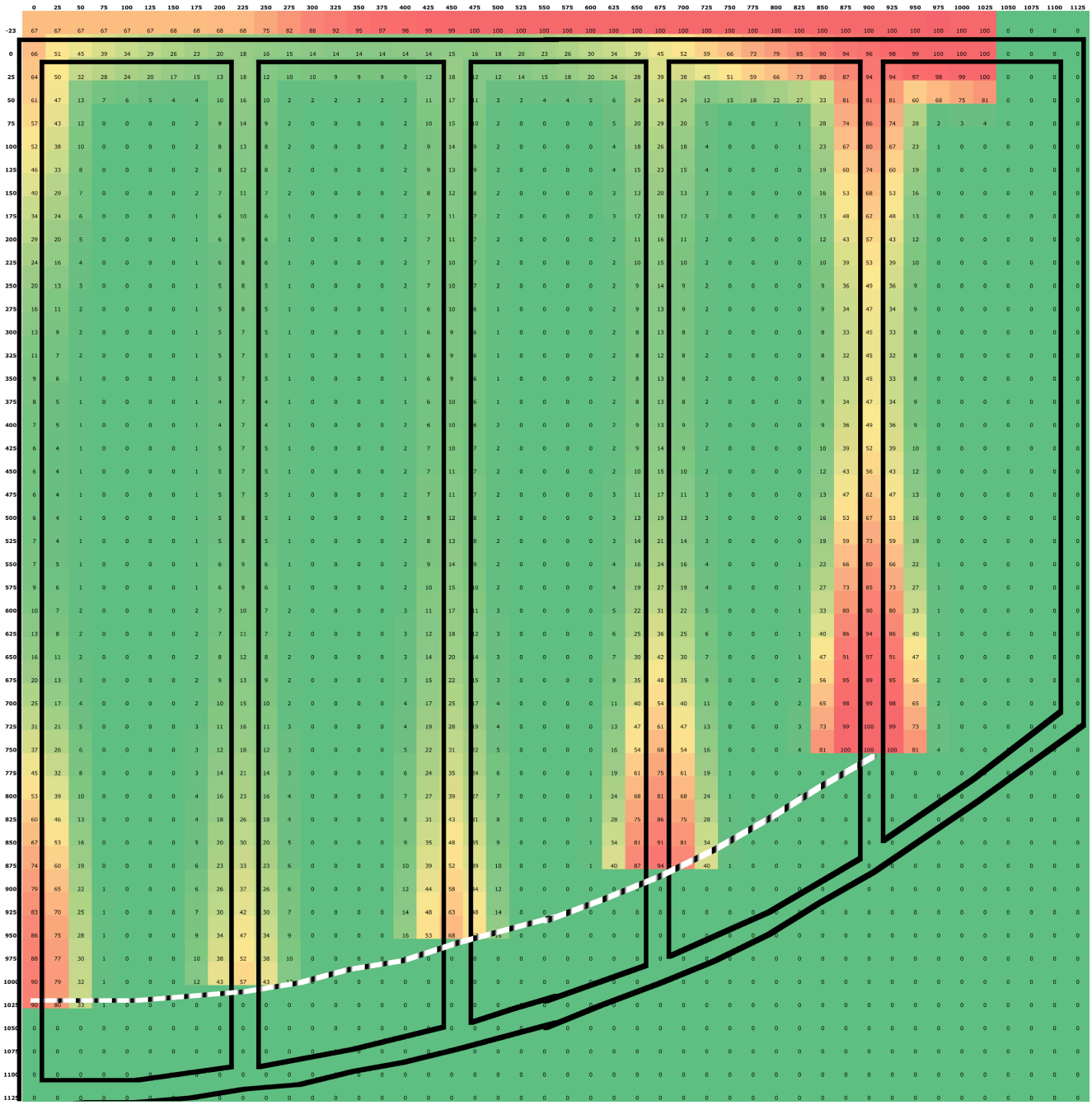

Figure 6-2
Mild Traumatic Brain Injury Risk Map based on the actual test results, for low Sea Lion tolerance to MTBI (1/3 Power Scaling Law)

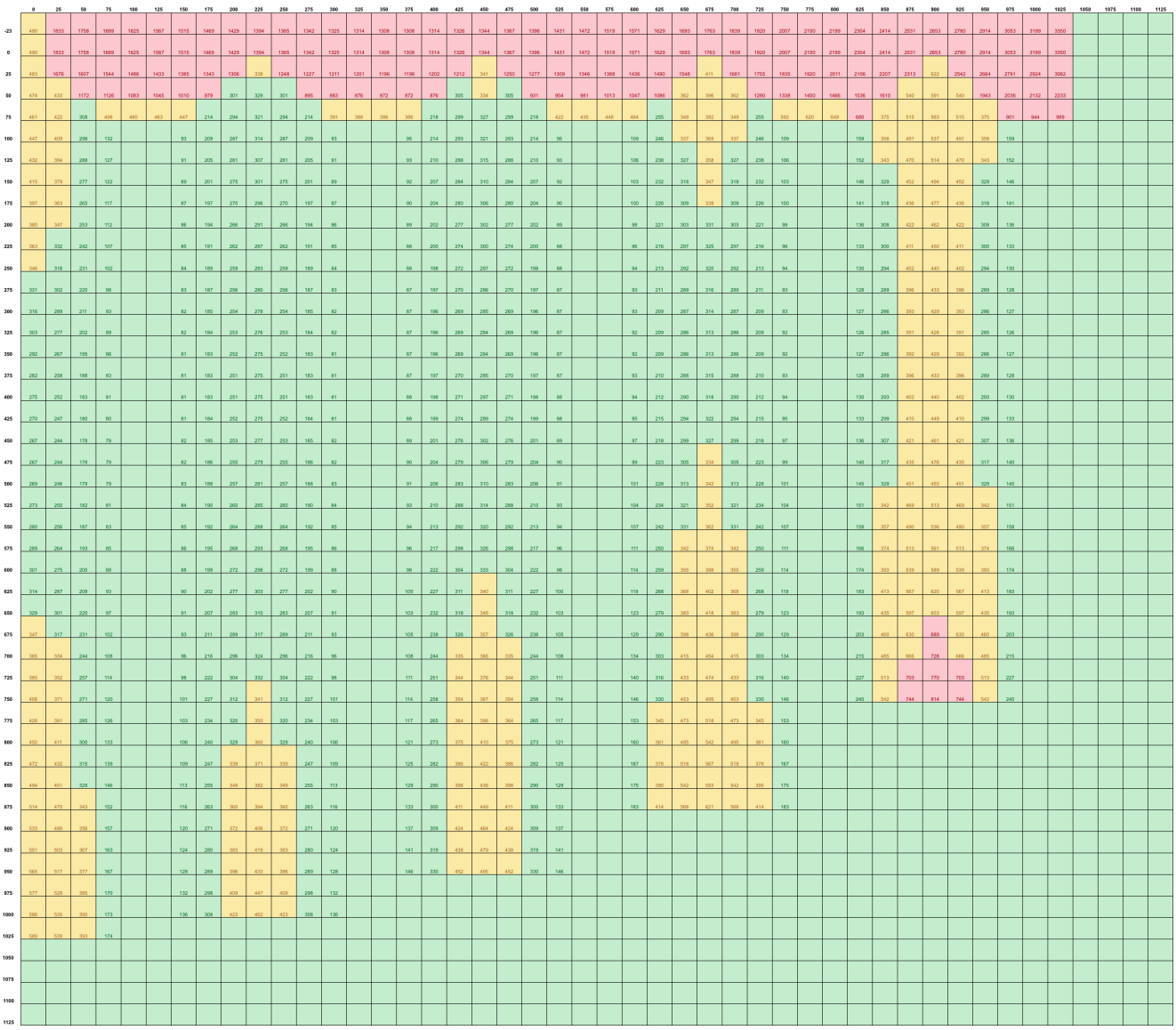

Figure 6-3
HIC map for the Grid, based on an impact angle of 45 degrees, impact speed 6.0 m/s, head mass 4.8 kg

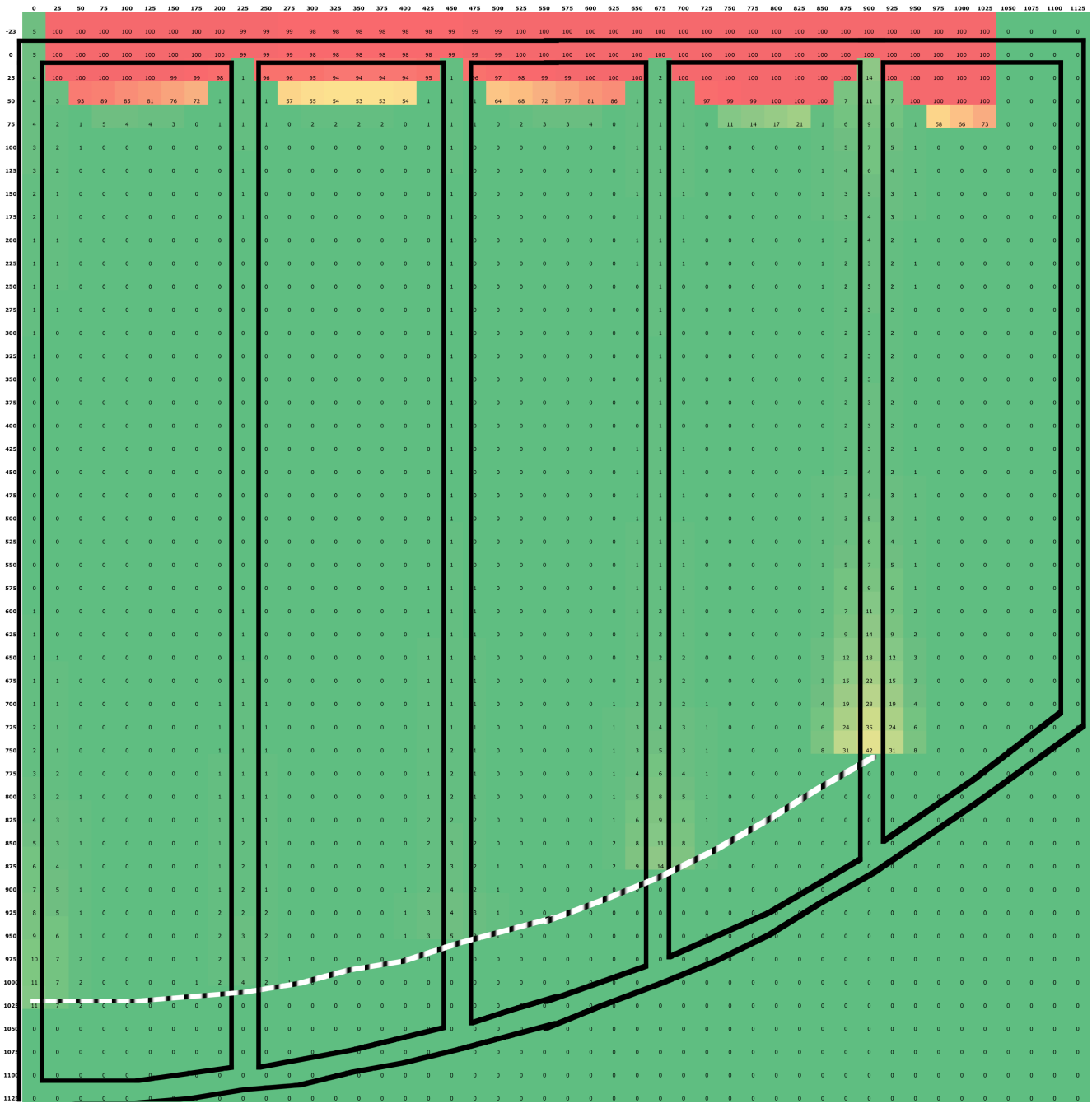

Figure 6-4
Mild Traumatic Brain Injury Risk Map based on an impact angle of 45 degrees, impact speed 6.0 m/s, head mass 4.8 kg, for low Sea Lion tolerance to MTBI (1/3 Power Scaling Law)

7 Summarising the Risk

In trawling, the grid is attached to, and surrounded by, netting. We have assumed that this limits the area over which interactions can take place. It has been assumed that the area 100 mm inside the outer edge of the grid will not interact with a sea lion during a trawl.

If the impacts with the locations in the interaction area are random, then the average HIC (and corresponding MTBI) can be calculated by averaging results over the remaining impact area. The average values for HIC and MTBI risk for a 90 degree impact and 45 degree impact are show in Table 7.1.

Table 7.1
Table of average and maximum values for HIC and MTBI at a 90 degree and a 45 degree impact angle

	90 degrees	45 degrees
Average HIC	550	415
Average Risk of MTBI (Impact Area)	18	11
Max HIC	1817	3350
Maximum Risk of MTBI	100	100

8 Discussion

This report documents the test methods, results and analysis used to create a 'map' of the likelihood of injury risk as a result of a head impact with a typical sea lion exclusion device (SLED) grid.

A number of tests were conducted at various locations on the structures that comprise the SLED grid to determine functions that could be used to estimate results at other locations not tested.

Some limitations were identified during the study that should be noted. During analysis, it become apparent that the accuracy of the results toward the outer edge of the grid might be improved with further tests at the extremity of the impact area. This would avoid the need to extrapolate results in these areas. Furthermore, the presence of rope binding at the centre of the grid affected the results. We expected to see a local minimum in the severity at this location, but the coupling of the two halves meant that this was not the case. Had the binding been replaced by a hammerlock, different results may have been obtained in this region.

Some further assumptions had to be made:

- That the impact response of the grid can be characterised as a spring. This assumption allowed results from perpendicular tests at 6.0 m/s with a 4.8 kg head impactor to be scaled for different impact speeds and masses using simple power relationships;
- That the effects of impact angle and impact offset, measured at one location, could be generalised to the entire grid. Furthermore, that the effect of impacts collinear with the centre of the horizontal bar (bar 12), but at an angle to the grid plane, could be estimated from previous tests on a different grid.
- Assumptions were also made about impacts within the corner areas of the grid, where simultaneous impact with two bars was likely.

Finally, the scaling of mild traumatic brain injury risk from a human brain injury risk has been estimated, and is of unknown validity. However, there are no other estimates of injury risk available.

Each of these assumptions can have an effect on the average MTBI risk.

The central rope binding affects the way the whole grid behaves in an impact. If the two grid halves were less tightly coupled (as was the case with the previous grid tested) the two grid halves would effectively behave independently of each other (except during an impact involving both central horizontal bars bar 12 and bar 13). Instead, the behaviour of the two grid halves were made dependent on each other due to the central rope binding, and results in this report are somewhat limited to a grid of this configuration.

Some additional testing of the risk model suggests that these two factors (the binding and the extrapolation) can have an affect on the estimates of the average MTBI. We understand that the model constructed in this study will be used in a meta-model of risk that will be used to guide decision-making in the management of the fishery. In the case that the meta-model would be substantively affected by a change in average MTBI risk, the authors suggest that some further testing take place: specifically, tests might be conducted at the outer edge of the contact zone, and the effect of replacing the binding with a hammerlock might be checked. Likewise, impacts within the corner areas may need to be considered further, as well as offset and angled impact tests at a number of different locations.

As it is, we feel that the balance of effects introduced by these factors is slightly overestimating the average risk, specifically if the use of rope binding to join the two halves of the grid is not usual practice.

The result of the testing and analysis is a spreadsheet model of MTBI risk that can be used in conjunction with the information on impact distributions over the grid area, impact speeds and angles, in models of risk arising from trawling operations. This report has specifically not estimated what those risks are, and the estimation of those risks using the model presented here remains to be determined.

Acknowledgements

This study was funded by the New Zealand Ministry of Fisheries, project number (SRP2010/05).

The authors wish to acknowledge the contributions of Dr Martin Cryer, Science Manager, Aquatic Environment, Ministry of Fisheries and Edward Abraham also of the Ministry of Fisheries, as well as members of the Aquatic Environment Working Group.

The authors wish to acknowledge the contributions of Daniel Searson, Research Engineer at the Centre for Automotive Safety Research.

The views expressed in this report are those of the authors and do not necessarily represent those of the University of Adelaide or the New Zealand Ministry of Fisheries.

References

Banerjee B, (2011) Review of CAR Report on impact characteristics of a SLED grid, Report for Deep Water Group Ltd, Industrial Research Limited, Auckland, New Zealand.

Funk JR, Duma SM, Manoogian SJ, Rowson S (2007) Biomechanical risk estimates for mild traumatic brain injury. Proceedings of the 51st Annual Scientific Conference for the Association for the Advancement of Automotive Medicine 2007, Melbourne, Australia.

Ponte G, van den Berg AL, Anderson RWG (2010) Impact characteristics of the New Zealand Fisheries sea lion exclusion device stainless steel grid Report for the Ministry of Fisheries, 15 October 2010 (Unpublished report held by Ministry of Fisheries, Wellington, New Zealand).

Searson DJ, (2011) The Influence of Test Conditions on the Results of Pedestrian Headform Impact Tests, PhD Thesis (Draft), The University of Adelaide.